

Southern Ocean response of CO₂ to increased Fe flux and effect on glacial atmospheric CO₂

A. J. Watson¹, D. C. E. Bakker¹, A. J. Ridgwell¹, P. W. Boyd² and C. S. Law³.

¹ School of Environmental Sciences, University of East Anglia, Norwich NR4 7TJ, UK

² NIWA Centre for Chemical and Physical Oceanography, Department of Chemistry, University of Otago, Dunedin, New Zealand

³ Centre for Coastal and Marine Studies, Plymouth Marine Laboratory, Prospect Place, The Hoe, Plymouth PL1 3DH, UK.

It has been postulated that utilization of carbon by the Southern Ocean biota is limited by iron^{1,2}. Greater Fe supply to the region in glacial time could have reduced atmospheric CO₂, and artificial Fe fertilization might increase carbon sequestration. In the first whole-ecosystem test of Southern Ocean iron limitation, we found surface fCO₂, and uptake ratios of silica to carbon, were strongly influenced by nanomolar changes in iron concentrations. We use these results to inform a model of global carbon and ocean nutrients, forced with atmospheric iron fluxes to the region derived from the Vostok³ core dust record. During glacial periods, predicted magnitudes and timings of atmospheric CO₂ changes match ice core records well. At the glacial terminations, the model suggests forcing of Southern Ocean biota by iron causes the initial ~40 ppm of glacial-interglacial CO₂ change, but other mechanisms must account for the remaining 40 ppm increase. Our experiment confirms that modest sequestration of atmospheric CO₂ by artificial Southern Ocean Fe fertilization is in principle possible, though the period and geographical extent over which sequestration would be effective remain poorly known.

The in-situ iron enrichment experiment was performed at 61°S, 141°W in February 1999⁴. The method was that of a tracer-steered iron release first described in ref 5 and previously employed in the equatorial Pacific^{6,7}. Ferrous sulphate solution in acidified seawater was released over a period of ~12 hours, in a region centred on a drogued drifting buoy, to create a patch of surface water, of linear dimensions ~10km, enriched to ~3 nM dissolved iron concentration. Sulphur hexafluoride (SF₆) tracer was released in a known ratio to iron in the initial release, enabling the subsequent advection and dilution of the patch to be accounted for. On days 4, 6 and 8 after the start of the experiment, when dissolved iron concentrations in the patch fell below ~0.3 nM, further additions of iron to the centre of the tracer-marked region were made.

Figure 1 shows the time sequence of surface water measurements of fCO₂ recorded on board the survey vessel during the 13 days of the experiment, as it moved continuously in and out of the enriched patch. The instrument and data reduction techniques used were similar to those described by Cooper *et al.*⁸. The increase with time, and much of the variability, of the “out of patch” fCO₂ is

largely accounted for by changes in temperature of the mixed layer, which warmed about 0.3°C during the period. The iron release changed the water from being approximately neutral with respect to atmospheric CO₂ to a sink, with surface water fCO₂ being ~30 μatm below the atmosphere in the patch at the end of the period. These are the first whole-ecosystem data which show that biologically mediated drawdown of surface fCO₂ is strongly responsive to the availability of iron in the polar Southern Ocean. Satellite observation of a feature, which we identify as the aftermath of the experiment six weeks after initial release, shows chlorophyll at concentrations similar to those which prevailed when we left the experiment at the end of two weeks, but in a patch covering 5-10 times the area at that time⁹. This suggests that

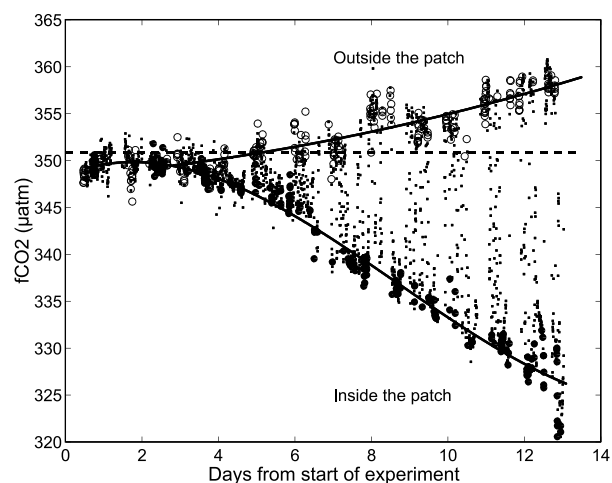


Figure 1. Seawater fCO₂ in surface water measured from the R/V *Tangaroa* as a function of time during the experiment. The simultaneously measured SF₆ tracer concentrations were used to construct the heavy lines, as follows: The “Outside patch” line is a quadratic fit to the set of data points having the lowest 10% of SF₆ concentrations (open circles), while the “inside patch” line is a cubic fitted to the set of points having the highest 10% SF₆ concentrations on each day (closed circles). The dotted line shows the mean of atmospheric fCO₂ measured during this period.

the sink for atmospheric CO₂ created by the iron release continued to grow in magnitude after we left the area.

The ratio of silicon to carbon fixed by the ecosystem is important for interpretations of the effect of iron fluxes on atmospheric CO₂ in glacial time, as indicated by model results reported here (see below, and supplementary information). Our measurements of the ratio of net uptake of silicon to carbon by the ecosystem showed a substantial response to iron addition, with the amount of silicon fixed per mole of carbon inside the patch being only about half that outside (see supplementary information). The ratio of uptake in the patch was established both by isotopic uptake incubations, and by examination of changes in bulk silicon and carbon concentration in the patch. Incubations taken from 5m depth show mean molar uptake ratios Si:C = 0.09 after day 5 of the experiment, while outside the patch the ratio was 0.17. Our observations are consistent with those recently reported in bottle Fe enrichment experiments in the Antarctic¹⁰ and elsewhere¹¹. When account is taken of the different variations with depth in the mixed layer of the silicon and carbon uptake rates (see supplementary information) we estimate 0.19 and 0.35 for respectively inside- and outside- patch Si:C over the mixed layer as a whole, values similar to the in-vitro observations. These are the first measurements to show an effect of iron on Si:C ratios in the unenclosed marine ecosystem.

What is the source of the iron needed by the Southern Ocean biota? It has generally been assumed^{1,12} that local atmospheric dust is the main source, but recent work has suggested instead that dissolved iron in upwelling water is more important¹³. Recent measurements indicate that the concentrations of dissolved iron in the Southern Ocean at depths of 800 m are ~0.3 nM far from land¹⁴, while surface water concentrations are limiting at ~0.05-0.1 nM. ¹⁴C tracer budgets¹⁵ and circulation models¹⁶ are in agreement about the magnitude of the upwelling flux of water (~20-40 Sv). From these figures we calculate a supply of iron by upwelling averaging 8-16 μmol m⁻² a⁻¹ for the ~2 x 10¹³ m² area south of the Polar front. Estimates for the source due to atmospheric dust vary. Both the dust flux itself, and the fraction of dissolvable iron it contains, are poorly constrained. Following data and assumptions of Duce and Tindale¹², Lefevre and Watson calculated a flux of 0.2 μmol m⁻² a⁻¹ dissolvable Fe for the Antarctic region¹⁵. 10% of the iron in the dust was assumed to be soluble. A recent modelling estimate of atmospheric dust fluxes¹⁷ suggests ~25 times higher dust flux to the region. However, recent work¹⁸ suggests that 10% solubility for the iron in dust is an order-of-magnitude overestimate. Thus, present-day upwelling flux appears to be on average larger, probably by an order of magnitude, than the atmospheric flux.

The extent of surface depletion of macro-nutrients is consistent with upwelled iron being the limiting nutrient in Southern Ocean waters. Laboratory measurement of the Fe requirements of open-ocean phytoplankton¹⁹ show that, under conditions in which oceanic diatoms are severely iron-stressed, their molar C:Fe uptake ratios rise to a maximum ~3 x 10⁵:1. This ratio implies that the maximum net drawdown due to iron-stressed plankton removing ~0.25

nM Fe from upwelled water should be ~75 μmol kg⁻¹ C, or (using C:N ~7) ~10 μmol kg⁻¹ nitrate. Typically nitrate concentrations in the region are indeed 10 μmol kg⁻¹ lower at the surface than at 800m²⁰.

Ice cores³, sediments² and models¹⁷ indicate that iron fluxes from the atmosphere were higher in glacial time by a factor of 2-5 globally, and 10-50 in the Southern Ocean. Therefore, during the glaciations, Southern Ocean atmospheric fluxes might have exceeded the upwelling source. This would result in a greater efficiency of the biological pump in the region. A similar increase in efficiency would be expected if the concentration of upwelling iron increased in response to global increases in the atmospheric source¹³.

Thus we might expect increased depletion of macro-nutrients during glacial time in this region, which could contribute to reduced atmospheric CO₂²¹. To quantitatively investigate the effect of Southern Ocean dust flux on these variables, we have adapted a simple model of the ocean-atmosphere carbon cycle, incorporating measured effects of iron on fCO₂ and silica-carbon ratios (see methods section and supplementary information). Figure 2 shows the result of driving the model with a variable dust deposition rate to the Southern Ocean based on the dust concentration record in the Vostok core, with all other model boundary conditions held constant. Variations in model atmospheric CO₂ during glaciated periods and in the first part of the four "terminations" match the ice core record well, as does the timing and approximate magnitude of the decrease in atmospheric δ¹³C in the initial stage of Termination I²² (not shown). Contrary to recent arguments that the delay between dust flux decline and atmospheric CO₂ change at Termination II is too long for the two to be directly linked via the Southern Ocean²³, we find the timings of events to be well-matched. As a result of a non-linear response of the system to changes in Fe supply, model CO₂ does not rise significantly until much of the decline in dust flux has taken place. The behaviour is a result of a shift from a glacial regime that is predominantly silicon limited to a modern one that is predominantly iron limited. The timing is sensitive to the forcing by dust flux, so that if the assumed present-day dust supply and/or the maximum glacial-interglacial change are significantly reduced, correlation between model and observed CO₂ signals at the Terminations is degraded, while if we had assumed a higher solubility for iron in dust we would have obtained a better match.

The maximum model [PO₄] drawdown in the Southern Ocean is ~0.6 μmol kg⁻¹, ~45% of that present at the surface of the Southern Ocean in the present day. This corresponds to an enhancement in the export flux of particulate organic matter (POM) of about 135%. This is consistent with proxy evidence in the Southern Ocean such as δ¹⁵N in organic matter, interpreted as indicating increased nutrient utilization at the Last Glacial Maximum (LGM)^{24,25}. Although diatoms account for over 90% of the model LGM increase in POM, inferred opal accumulation rates in the real ocean suggest relatively little overall increase in opal export at this time²⁶. These apparently conflicting signals may be reconciled if there is more efficient use of silicate by

diatoms as a result of increased Fe availability. Indeed, the model increase in opal export is only $\sim 40\%$, less than a third that exhibited by POM. Thus glacial/interglacial variability in the strength of biological surface silicon and carbon depletions is fundamentally de-coupled by changes in Fe supply.

The amplitude of $x\text{CO}_2$ change predicted by the model is limited to about 45 ppm. Of this ~ 35 ppm is through a ‘fast’ response of biological productivity to increased Fe availability, consistent with earlier models¹³. This is due to the lowering of Southern Ocean surface $f\text{CO}_2$, which is ~ 60 uatm in the model, of the same order as the SOIREE patch may have finally obtained. About 10 ppm of the model response occurs more gradually, as a lagged response of the system arising from ‘calcium carbonate compensation’¹⁵. By

altering the parameterization of diatom cellular Si:C ratios it is possible to make the dust signal drive more of the CO_2 rise at the terminations. However, Cd/Ca proxy evidence constrain productivity changes to be relatively modest²⁷. We therefore believe it most likely therefore that one or more additional mechanisms to increase the concentration of atmospheric CO_2 must cut in once the termination is underway to account for the observed deglacial increase of around 80 ppmv [REF: 3]. Possible candidates at the deglaciation include other Southern Ocean mechanisms such as changes in sea ice extent²⁸, mixing²⁹ and surface stratification^{24,25}.

Models of the processes influencing atmospheric CO_2 indicate that carbon might be sequestered from the atmosphere for long periods (ie. centuries or longer) by

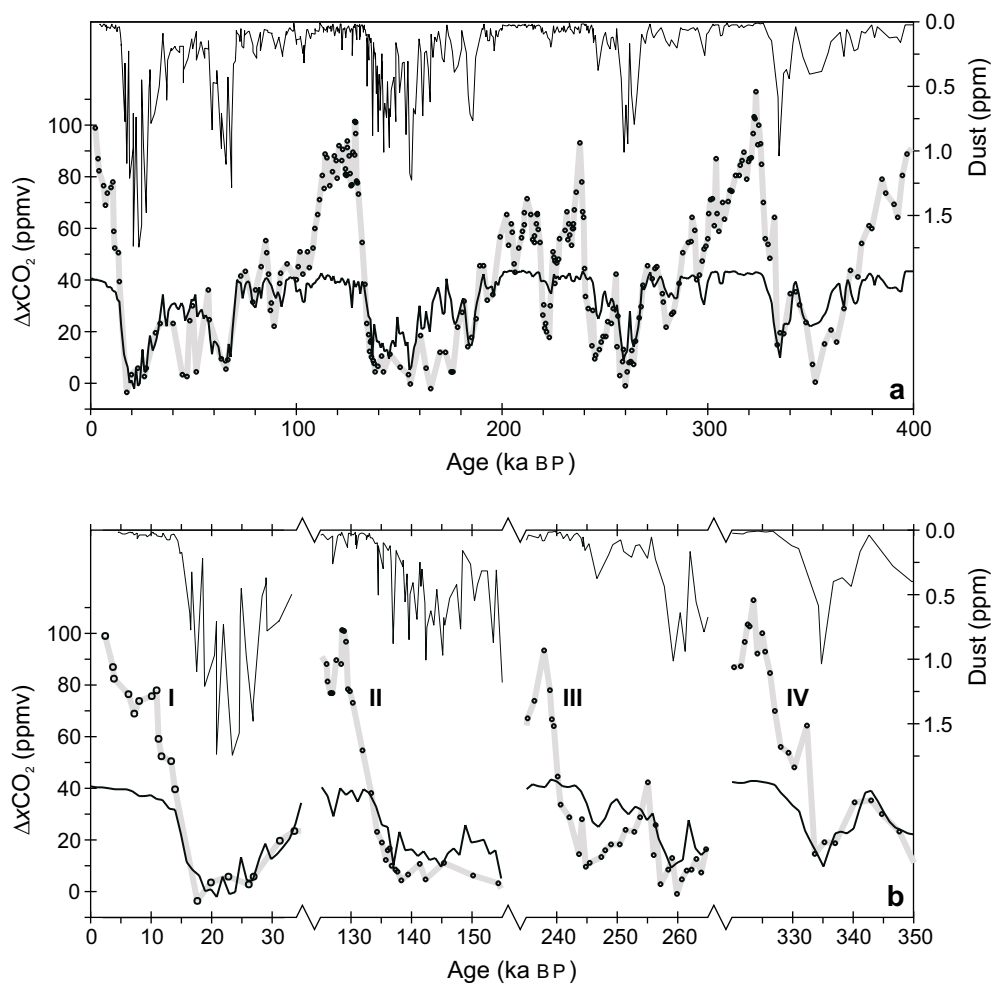


Figure 2. Comparison between the Vostok ice core record³ of atmospheric CO_2 and the atmospheric CO_2 concentration from our carbon cycle model, forced only by changing Southern Ocean dust fluxes. (a) The Vostok core dust record (inverted, at top), is used to force the model. The Vostok CO_2 record (thick grey line) is compared to the model atmospheric CO_2 (black line). The ice core data are plotted using the age models described in ref 3. The observed and model CO_2 records are plotted as deviations from their LGM value ($\Delta x\text{CO}_2$). CO_2 levels in the model remain weakly sensitive to iron fluxes even when Fe is abundant in glacial times, due to the dependence of Si:C ratios on Fe concentrations. (b). Sections of the plot in (a) covering the four terminations (labeled ‘I’ through ‘IV’) on a magnified time scale to better show the timing between of observed and model CO_2 records.

deliberate fertilization of the Southern Ocean, though early suggestions that this would sequester carbon rapidly enough to substantially slow the rise of atmospheric CO₂ have been shown to be incorrect³⁰. Our observations confirm that stimulation of the Southern Ocean carbon fixation is possible using iron addition. Integration of the deficit in dissolved inorganic CO₂ signal gives 1200 (\pm 10%) tonnes of excess C photosynthetically fixed in the patch by day 12, larger than the independent estimate of extra algal carbon biomass⁴. However, our estimates of the amount removed from the atmosphere by the SOIREE bloom remain uncertain. No enhanced export flux was detected during the first 13 days of the experiment⁴. If the bloom we induced eventually produced enhanced export, or the water at the surface was subducted on a timescale of a year or less, similar amounts could be sequestered from the atmosphere for long periods, though semi-continuous fertilization might be needed to achieve lasting sequestration³⁰. Otherwise, if there was no enhanced sinking flux, the phytoplankton biomass was re-mineralized in the surface water and this remained at the surface without subduction, carbon taken up from the atmosphere would be returned there on a time scale of a year or so.

Methods: Ocean-atmosphere carbon cycle box model.

The ocean-atmosphere carbon cycle model is based on a simplified representation of ocean circulation previously used in carbon cycle investigations^{24,25,31}. Tracers advected in the ocean component include total dissolved inorganic carbon (Σ CO₂), dissolved oxygen (O₂), alkalinity, temperature and salinity. Of these, CO₂ and O₂ are exchanged with a 'well-mixed' atmosphere across the air-sea interface. The stable isotopes of carbon (¹²C and ¹³C) are treated separately, with all significant fractionation processes between them taken into account.

We describe the elements of the biological model briefly here, and in more detail in the supplementary information. Three nutrients potentially limiting to biological activity in the ocean are considered; phosphate (PO₄), silicic acid (H₄SiO₄), and total dissolved iron (Fe). The export of particulate organic matter (POM) from the surface ocean is estimated directly from ambient concentrations of these nutrients (and further modified to reflect temperature and insolation effects). This is a common simplification in global carbon cycle models, circumventing the need for a full ecological model in the euphotic zone. We explicitly consider export arising from two distinct phytoplankton classes; diatoms and non-diatoms. Diatom productivity is assumed to be responsible for the export of opal, and is sensitive to the availability of H₄SiO₄. In contrast, non-diatom productivity is assumed to be responsible for the export of CaCO₃ (at a constant fraction), and is not directly influenced by ambient [H₄SiO₄]. Both classes contribute to export of POM, and as such share a common control by PO₄ and Fe availability.

Net Fe:C uptake ratios in both phytoplankton classes, and Si:C in diatoms, are varied as a function of [Fe]. In the former case the dependence of this ratio on Fe availability is derived empirically from incubation results⁹. In the latter, we use changes in this ratio between Fe-replete and Fe-depleted conditions observed during this and previous studies^{10,11}. A continuous function for the Si:C ratio under intermediate degrees of Fe-limitation is constructed based on the assumption that, while the production rate of organic material is increasingly restricted with decreasing Fe-availability, the rate of deposition of opal in diatoms is comparatively invariant (see supplementary information). The assumption is made in our model that changes in phytoplankton Fe:C and Si:C ratios are reflected

proportionally in final export ratios. The composition of POM is characterized by a fixed ratio of C:N:P.

The biogeochemical cycling of dissolved iron in the ocean is treated in a similar manner to recent modelling work¹³. However, we assume that the scavenging rate of iron is proportional to the flux of particulate material falling through the water column, and do not account for the action of Fe-binding ligands. Particulate material exported from the euphotic zone is partially remineralized/dissolved within the water column. For simplicity, all POM and opal reaching the deep-sea sediment is returned in dissolved form to the ocean. An exception is made for Fe compounds (and complexes), which are removed from the system in order to balance their aeolian input at the ocean surface. The net accumulation of CaCO₃ in sediments is estimated as a function of deep-water chemical conditions, CaCO₃ and POM rain rates, and sedimentary CaCO₃ content³². The ocean-atmosphere system is therefore 'closed' with respect to PO₄ and H₄SiO₄ (and O₂), but 'open' with respect to CO₂, alkalinity, and Fe.

In order to obtain the results shown in Figure 2 the model was configured for the present-day carbon cycle, using distributions of dust deposition taken from GCM simulations¹⁷. Fe is assumed to constitute 3.5% (by mass) of the dust flux, of which 2% is soluble in the Southern Ocean. Biological productivity and Fe scavenging schemes were 'tuned' to give a reasonable match of model ocean distributions of [PO₄], [H₄SiO₄], and [Fe] to observations, together with realistic deep-sea particulate matter rain rates. After 'spin-up', the model was run for 400 ka, with the dust deposition flux to the Southern Ocean varied according to the Vostok dust concentration signal³. The dust flux was scaled so that the maximum value at the LGM was 25 times that for the present-day, consistent with model estimates for the Southern Ocean deposition¹⁷. No other model boundary conditions were changed.

References

- Martin, J. H. Glacial-interglacial CO₂ change; the iron hypothesis. *Paleoceanogr.* **5**, 1-13 (1990).
- Kumar, N. *et al.* Increased Biological Productivity and Export Production In the Glacial Southern-Ocean. *Nature* **378**, 675-680 (1995).
- Petit, J. R. *et al.* Climate and Atmospheric History of the Past 420 000 years from the Vostok Ice Core, Antarctica. *Nature* **399**, 429-436 (1999).
- Boyd, P. W. *et al.* Phytoplankton bloom upon mesoscale iron fertilisation of polar Southern Ocean waters. *Nature* (Submitted).
- Watson, A. J., Liss, P. S. & Duce, R. A. Design of a small scale iron enrichment experiment. *Limn. Oceanogr.* **36**, 1960-1965 (1991).
- Martin, J. H. *et al.* Testing the Iron Hypothesis In Ecosystems Of the Equatorial Pacific- Ocean. *Nature* **371**, 123-129 (1994).
- Coale, K. H. *et al.* A Massive Phytoplankton Bloom Induced By an Ecosystem-Scale Iron Fertilization Experiment In the Equatorial Pacific-Ocean. *Nature* **383**, 495-501 (1996).
- Cooper, D. J., Watson, A. J. & Ling, R. D. Variation of P-CO₂ along a North Atlantic shipping route (UK to the Caribbean): A year of automated observations. *Mar. Chem.* **60**, 147-164 (1998).
- Abraham, E. R., *et al.* The stirring of an iron-fertilised phytoplankton bloom. *Nature* (submitted).
- Takeda, S. Influence of iron availability on nutrient consumption ratio of diatoms in oceanic waters. *Nature* **393**, 774-777 (1998).
- Hutchins, D. A. & Bruland, K. W. Iron-limited diatom growth and Si:N uptake ratios in a coastal upwelling regime. *Nature* **393**, 561-564. (1998).
- Duce, R. A. & Tindale, N. W. Atmospheric Transport of Iron and Its Deposition in the Ocean. *Limnol. Oceanogr.* **36**, 1715-1726 (1991).
- Lefevre, N. & Watson, A. J. Modelling the geochemical cycle of iron in the oceans and its impact on atmospheric carbon dioxide concentrations. *Glob. Biogeochem. Cyc.* **13**, 727-736 (1999).
- Sohrin, Y. *et al.* The distribution of Fe in the Australian sector of the Southern Ocean. *Deep-Sea Res.* pt 1. **47**, 55-84 (2000).

15. Broecker, W. S. & Peng, T., -H. The role of CaCO₃ compensation in the glacial to interglacial atmospheric CO₂ change. *Glob. Biogeochem. Cyc.* **1**, 15-29 (1987).
16. Stevens, D. P. & Ivchenko, V. O. The zonal momentum balance in an eddy-resolving general-circulation model of the Southern Ocean. *Quart. J. Roy. Met. Soc.* **123**, 929-951 (1997).
17. Mahowald, N. *et al.* Dust sources and deposition during the last glacial maximum and current climate: a comparison of model results with paleodata from ice cores and marine sediments. *J. Geophys. Res. - atmospheres.* **104**, 15895-15916 (1999).
18. Jickells, T. D. & Spokes, L. J. in *The biogeochemistry of iron in seawater* (eds. Turner, D. R. & Hunter, K. A.) (John Wiley, New York, in press).
19. Sunda, W. G. & Huntsman, S. A. Iron Uptake and Growth Limitation In Oceanic and Coastal Phytoplankton. *Mar. Chem.* **50**, 189-206 (1995).
20. Levitus, S., Burgett, R. & Boyer, T. *World Ocean Atlas 1994 vol 3: Nutrients* (NOAA Atlas NESDIS 3, US Dept of Commerce, Washington D.C., 1994).
21. Sarmiento, J. L. & Toggweiler, J. R. A New Model For the Role Of the Oceans In Determining Atmospheric Pco₂. *Nature* **308**, 621-624 (1984).
22. Smith, H. J., Fischer, H., Wahlen, M., Mastroianni, D. & Deck, B. Dual modes of the carbon cycle since the Last Glacial Maximum. *Nature* **400**, 248-250 (1999).
23. Broecker, W. S. & Henderson, G. M. The sequence of events surrounding Termination II and their implications for the cause of glacial-interglacial CO₂ changes. *Paleoceanogr.* **13**, 352-364 (1998).
24. Francois, R. *et al.* Contribution of Southern Ocean surface-water stratification to low atmospheric CO₂ concentrations during the last glacial period. *Nature* **389**, 929-935 (1997).
25. Sigman, D. M., Altabet, M. A., Francois, R., McCorkle, D. C. & Gaillard, J. F. The isotopic composition of diatom-bound nitrogen in Southern Ocean sediments. *Paleoceanogr.* **14**, 118-134 (1999).
26. Mortlock, R. A. *et al.* Evidence for lower productivity in the Antarctic Ocean during the last glaciation. *Nature* **351**, 220-222 (1991).
27. Rickaby, R. E. M. & Elderfield, H. Planktonic foraminiferal Cd/Ca: Paleonutrients or paleotemperature? *Paleoceanogr.* **14**, 293-303 (1999).
28. Stephens, B. B. & Keeling, R. F. The influence of Antarctic sea ice on glacial-interglacial CO₂ variations. *Nature* **404**, 171-174 (2000).
29. Toggweiler, J. R. Variation of atmospheric CO₂ by ventilation of the ocean's deepest water. *Paleoceanogr.* **14**, 571-588 (1999).
30. Peng, T. H. & Broecker, W. S. Dynamic Limitations On the Antarctic Iron Fertilization Strategy. *Nature* **349**, 227-229 (1991).
31. Keir, R. S. On the late Pleistocene ocean geochemistry and circulation. *Paleoceanogr.* **3**, 413-445 (1988).
32. Archer, D. Modeling the calcite lysocline. *J. Geophys. Res.* **96**, 17037-17050, (1991).

Acknowledgements

We thank Kim Tanneburger, Ute Schuster, and the officers and crew of the R/V *Tangaroa* for their support. This work was made possible by grants from the United Kingdom Natural Environment Research Council and the New Zealand National Institute for Water and Atmospheric Research. We acknowledge support from the CEFIC iron salts committee.

Supplementary information 1:

Estimates of silica-to-carbon uptake and export ratios during SOIREE

A. J. Watson¹, D. C. E. Bakker¹, A. J. Ridgwell¹, P. W. Boyd² and C. S. Law³.

¹ School of Environmental Sciences, University of East Anglia, Norwich NR4 7TJ, UK

² NIWA Centre for Chemical and Physical Oceanography, Department of Chemistry, University of Otago, Dunedin, New Zealand

³ Centre for Coastal and Marine Studies, Plymouth Marine Laboratory, Prospect Place, The Hoe, Plymouth PL1 3DH, UK.

We have two sources of information on the net ecosystem uptake ratio of silica to carbon:

(1) Incubation experiments using radioisotopes ¹⁴C and ³²Si.

¹⁴C measurements were made throughout the experiment at a number of depths both inside and outside the fertilised patch. We have a limited number of ³²Si measurements, made using the method of ref 1, at a single depth (5m), and mostly inside the patch. Duplicate determinations of silicon uptake, and triplicate determinations of ¹⁴C uptake, were made from each sample. Standard deviations of these replicates were typically ~3% for ³²Si and ~10% for ¹⁴C at 5m.

Table I shows the mole ratio of ³²Si and ¹⁴C uptake rates from paired incubations at 5m during the experiment. The mean of the in-patch ratios and out of patch ratios are respectively 0.09 and 0.17, confirming in an un-enclosed system the decrease in silicon to organic matter ratios of about a factor of two seen by earlier authors using bottle iron-enrichments^{2,3}. A t-test (one-tailed, homoscedastic) of the in-patch and out-of-patch samples shows that their means are significantly different at the $\alpha = 0.02$ level.

Carbon fixation rates are a function of both algal biomass and light intensity. There is no direct requirement for light in silicon uptake, but the cells must be actively growing to incorporate silicon. Thus we expect silicon uptake to occur throughout the euphotic zone but not to scale directly with light intensity, and to first order might expect it to be constant per cell through the mixed layer since there was significant primary production throughout this region. In order to extrapolate the measured silica fixation rates to the mixed layer as a whole, we assumed that they were proportional to the measured biogenic silica (a measure of the diatom biomass) at each depth, but otherwise independent of depth. Using this assumption silica fixation rates integrated through the mixed layer were calculated. The ratio of these to the measured integrated ¹⁴C primary production rates through the mixed layer gives an estimate of the overall Si:C ratio. The mean of the in-patch Si:C was 0.19 by this method, while the out of patch value was 0.35. These estimates are similar to the values that would be expected from the Si:N uptake ratios in bottle Fe enrichments from the Southern Ocean reported by Takeda².

(2) Bulk measurements of variations in silicate and ΣCO_2 .

Inside the patch, net uptake of nutrients and carbon was evident in the decline in the concentrations of the dissolved phase over the two weeks of the experiment. From the 12th to the 22nd of February (days 3 to 13 of the experiment), silicate declined by 2.5 $\mu\text{mol kg}^{-1}$ and ΣCO_2 by 15.6 $\mu\text{mol kg}^{-1}$ in the centre of the patch in the top 20m, suggesting an uptake ratio of 0.16, in reasonable agreement with the mean of the “normalized” in-patch incubations given above.

References

1. Brzezinski, M.A., Phillips, D.R., 1997. Evaluation of ³²Si as a tracer for measuring silica production rates in marine waters. *Limnol. Oceanog.* **42**, 856-865.
2. Takeda, S. Influence of iron availability on nutrient consumption ratio of diatoms in oceanic waters. *Nature* **393**, 774-777 (1998).
3. Hutchins, D. A. & Bruland, K. W. Iron-limited diatom growth and Si:N uptake ratios in a coastal upwelling regime. *Nature* **393**, 561-564. (1998).

Table I Si:C ratios at 5m depth during SOIREE

	Day from start of the experiment	Si:C (mol:mol)
In patch		
	5	0.12
	7	0.07
	9	0.10
	10	0.07
	11	0.04
	12	0.09
	13	0.16
mean		0.093
standard deviation		0.039
Out of patch		
	3	0.18
	5	0.16
mean		0.17
standard deviation		0.014

Supplementary information 2:

Model description

A. J. Watson¹, D. C. E. Bakker¹, A. J. Ridgwell¹, P. W. Boyd² and C. S. Law³.

¹ School of Environmental Sciences, University of East Anglia, Norwich NR4 7TJ, UK

² NIWA Centre for Chemical and Physical Oceanography, Department of Chemistry, University of Otago, Dunedin, New Zealand

³ Centre for Coastal and Marine Studies, Plymouth Marine Laboratory, Prospect Place, The Hoe, Plymouth PL1 3DH, UK.

Introduction

The ocean-atmosphere carbon cycle model is based on a highly simplified representation of mean annual ocean circulation, ideal for long-term simulation studies. Tracers advected in the ocean component include total dissolved inorganic carbon (DIC), dissolved oxygen (O₂), alkalinity (ALK), temperature and salinity. Of these, carbon (as CO₂) and O₂ are exchanged with a ‘well-mixed’ atmosphere across the air-sea interface. The biogeochemical cycling of three nutrients potentially limiting to biological activity in the

ocean is considered; phosphate (PO₄), silicic acid (H₄SiO₄), and dissolved iron (Fe). Particulate biogenic material is exported from surface ocean layers and partly remineralized within the water column. Material reaching the ocean floor interacts with the sediments there, and may be buried or returned in dissolved form back to the ocean. The two stable isotopes of carbon (¹²C and ¹³C) are treated separately, with all significant fractionation processes involving the transformation of carbon taken into account. Model biogeochemical cycling is shown schematically in Figure 1.

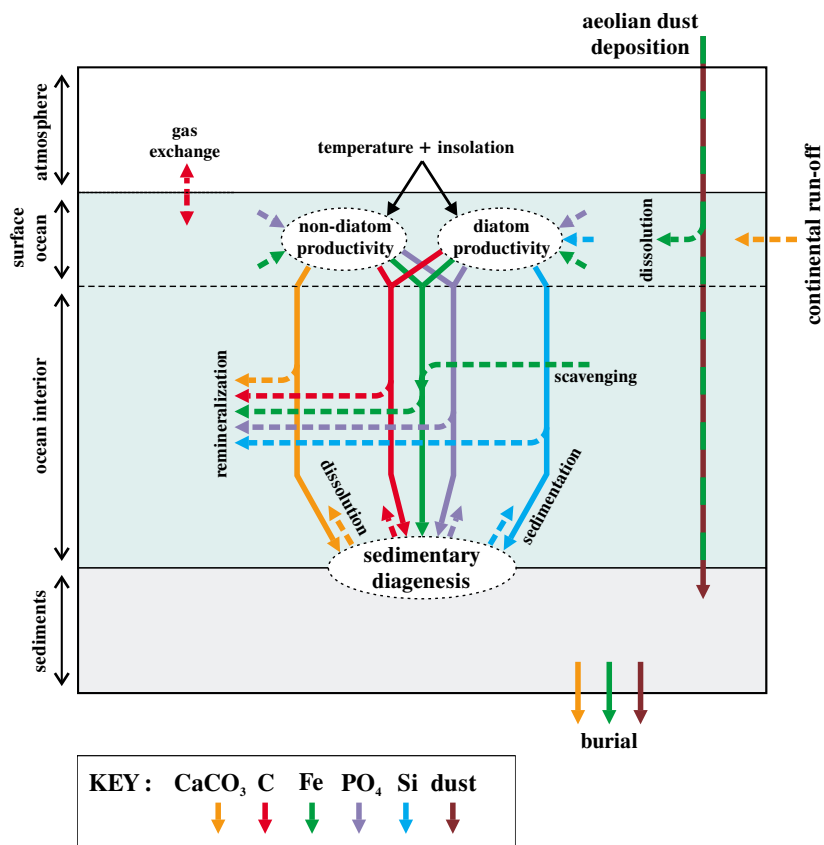


Figure 1 Model biogeochemical cycling schematic

Ocean configuration and circulation

The basic physical structure of the ocean follows that of the ‘‘CYCLOPS’’ box-model¹. This considers 6 distinct oceanic regions, divided vertically into surface, intermediate, and deep layers (except in the North Atlantic and Southern Ocean where the intermediate and deep layers are considered as one), giving a total of 16 separate homogeneous boxes. Ocean circulation (both advective and mixing flows) is prescribed after ref 1.

Ocean floor is defined within each region according to a (global mean) hypsographic curve². This profile is discretized into a series of depth bands down to a maximum depth of 6000 m, each spanning an interval of 500 m in the deep ocean but with an increasing resolution towards the ocean surface. Ocean-sediment interactions are calculated separately for each depth band, and within each ocean region.

Surface forcings

In order to calculate surface forcings required by the model, latitudinal and longitudinal boundaries are prescribed for each of the 6 ocean regions. These boundaries are used in conjunction with global gridded data sets to produce mean values for each region. For SST and SSS these are derived from Levitus³ and for dust deposition from GCM simulations⁴. Mean annual insolation is calculated at the mid-latitude of each region. Surface forcing values for each region are detailed in Table 1.

Gas exchange

The exchange of CO₂ between the ocean surface and atmosphere is estimated with a gas transfer coefficient of 0.06 mol m⁻² μatm⁻¹ yr⁻¹⁵ and via a representation of the aqueous carbonate system similar to ref 6. The concentration of O₂ in the surface ocean is assumed to always be in equilibrium with the atmosphere⁵.

Biological production

In the manner in which it seeks to estimate export production from the euphotic zone directly from surface physical and chemical conditions (rather than via a computationally-expensive ecosystem model), the scheme for surface ocean biological production is very similar to that of ref 5. However, we depart from this in that we consider production arising from two distinct classes of phytoplankton; diatoms and non-diatoms. Both classes are responsible for the production of particulate organic matter (POM), and as such, are limited by the availability of PO₄ and Fe. Diatoms are assumed to be responsible for the production of opal and are therefore limited by the availability of H₄SiO₄. In contrast, non-diatoms (such as coccolithophorids) have no such silicic acid limitation, but are assumed to be the sole producers of calcium carbonate (CaCO₃). Since in the absence of any nutrient limitation diatoms tend to dominate oceanic systems, they are characterized in the model by relatively high net productivity. Non-diatoms, comprising generally smaller species more tightly controlled by grazing activity, are characterized by much lower net productivity. Although this is an extremely simplistic treatment, with no explicit representation of the action of either zooplankton or the microbial loop, we find that such a scheme is still able to capture the first order contrast in observed calcium carbonate to particulate organic matter rain ratio (CaCO₃:POC) between different oceanic regions.

Phosphate export model

Net uptake of PO₄ (in units of mol PO₄ kg⁻¹ a⁻¹) within the euphotic zone for diatoms ($U_D^{PO_4}$) and non-diatoms ($U_{ND}^{PO_4}$) is described by

$$U_D^{PO_4} = U_{0,D}^{PO_4} \cdot \mu_{(I)} \cdot \mu_{(T)} \cdot \text{MIN}\left(k_D^{PO_4}, k_D^{H_4SiO_4}, k_D^{Fe}\right) \quad (1)$$

$$U_{ND}^{PO_4} = U_{0,ND}^{PO_4} \cdot \mu_{(I)} \cdot \mu_{(T)} \cdot \text{MIN}\left(k_{ND}^{PO_4}, k_{ND}^{Fe}\right) \quad (2)$$

Table 1 Surface Ocean Forcing Details

Surface region ¹	Surface area (m ²)	Temperature ² (°C)	Salinity ² (‰)	Relative insolation	Dust flux ³ (g m ⁻² a ⁻¹)	Dust flux ⁴ (g m ⁻² a ⁻¹)	Fe solubility (%)
Boreal	0.35×10 ¹³	2.9	34.3	0.35	0.47	0.47	0.5
Atlantic	7.35×10 ¹³	19.6	35.8	0.84	5.57	5.57	0.5
Antarctic	3.85×10 ¹³	2.4	34.0	0.44	0.14	3.45	2
Indian	5.95×10 ¹³	22.8	35.0	0.82	5.25	5.25	0.5
South Pacific	8.75×10 ¹³	21.8	35.2	0.77	0.26	0.26	1
North Pacific	8.75×10 ¹³	22.2	34.4	0.76	0.22	0.22	1

¹ see Keir [1988]

² from Levitus et al. [1994]

³ from Mahowald et al. [1999] - present-day simulation

⁴ from Mahowald et al. [1999] - LGM simulation (modified climate and dust sources)

where $U_{0,D}^{\text{PO}_4}$ and $U_{0,ND}^{\text{PO}_4}$ are uptake rates ($\text{mol PO}_4 \text{ kg}^{-1} \text{ a}^{-1}$) for the respective phytoplankton classes in the absence of any nutrient limitation, $\mu_{(I)}$ is a normalized factor accounting for the first-order effect on new production of solar insolation (Table 1), and $\mu_{(T)}$ is a modifying factor accounting for the influence of temperature, characterized by a value of 1.0 at 0°C with a Q_{10} of 1.88⁷. Due to the highly simplified nature of the physical ocean representation, no account can be made of the effect of mixed-layer depth on biological productivity. The k terms in (1) represent a Michaelis-Menten type kinetic limitation of uptake, defined

$$k_D^{\text{PO}_4} = \frac{[\text{PO}_4]}{K_{S,D}^{\text{PO}_4} + [\text{PO}_4]} \quad (3a)$$

$$k_D^{\text{H}_4\text{SiO}_4} = \frac{[\text{H}_4\text{SiO}_4]}{K_{S,D}^{\text{H}_4\text{SiO}_4} + [\text{H}_4\text{SiO}_4]} \quad (3b)$$

$$k_D^{\text{Fe}} = \frac{[\text{Fe}]}{K_{S,D}^{\text{Fe}} + [\text{Fe}]} \quad (3c)$$

where K_S is a half-saturation constant. The non-diatom terms are similar, except there is no H_4SiO_4 limitation.

At steady state, export production out of the euphotic zone is simply equal to net uptake, so that total PO_4 export out of each surface ocean box (in units of $\text{mol PO}_4 \text{ a}^{-1}$) is obtained by scaling the uptake rates calculated by (1) and (2) by the mass of each box. Exported organic matter is assumed to be entirely in particulate form.

Nutrient half-saturation constants

The PO_4 half saturation constant for diatoms is taken from ref 8. On the basis that coccolithophorids have been observed to exhibit a higher affinity for phosphate than do diatoms^{9,10}, non-diatoms are assigned a value 50% lower.

The value for the H_4SiO_4 half saturation constant for diatoms is taken to be $4 \mu\text{mol kg}^{-1}$, consistent with values reported from kinetic experiments on individual species and natural assemblages^{11,12}.

The value for the Fe half saturation constant for diatoms follows that observed in *T. oceanica*, while non-diatoms follows that for *E. huxleyi*¹³. The theoretical Fe' scale calculated by ref 13 is converted to the total dissolved scale used in the model by assuming that Fe' represents about 4% of total dissolved Fe in sunlight surface waters¹⁴.

Values for the nutrient half-saturation constants are summarized in Table 2.

'Redfield' and derived chemical export ratios

The relative proportions of C and PO_4 in POM follow the 'classic' Redfield ratio of 106:1. Although NO_3 is not explicitly considered in our model it does play a part in alkalinity cycling, and is therefore assumed present in POM set at a ratio with PO_4 of 16:1. Finally, oxygen is released through net biological production in the surface ocean and consumed via remineralization in the interior, both in a ratio with PO_4 of 177:1.

CaCO_3 is exported in a fixed ratio ($r_{0,ND}^{\text{CaCO}_3:\text{C}}$) with non-diatom particulate organic carbon (POC). Variability in

Table 2 Values of the Nutrient Half-saturation Constants for the Two Phytoplankton Groups

Phytoplankton group	Nutrient	K_S value
Diatoms	PO_4	$0.12 \mu\text{mol kg}^{-1}$
Diatoms	H_4SiO_4	$4.0 \mu\text{mol kg}^{-1}$
Diatoms	Fe	$0.08 \text{ nmol kg}^{-1}$
Non-diatoms	PO_4	$0.06 \mu\text{mol kg}^{-1}$
Non-diatoms	H_4SiO_4	n/a
Non-diatoms	Fe	$0.04 \text{ nmol kg}^{-1}$

the overall $\text{CaCO}_3:\text{POC}$ rain ratio can therefore arise through changes in the balance of export production between diatoms and non-diatoms. For instance, in the model Antarctic where H_4SiO_4 is not limiting to diatoms at present $\text{CaCO}_3:\text{POC}$ is low, whereas in the Atlantic where diatoms are limited by $[\text{H}_4\text{SiO}_4]$, non-diatoms are enabled in playing a much greater role, resulting in high $\text{CaCO}_3:\text{POC}$.

Cellular $\text{Fe}:\text{C}$ is assumed to increase with the availability of Fe following ref 13. Two empirical relationships are constructed, one for each phytoplankton class. In these, diatoms follow the observed behaviour of *T. oceanica* while non-diatoms follow *E. huxleyi*¹³. The theoretical Fe' scale ref 13 is converted to the model total dissolved Fe scale as outlined previously, to give

$$r_D^{\text{Fe}:\text{C}} = \frac{1}{\text{MIN}(300000, 15000 + 115623 \cdot ([\text{Fe}] - 0.125)^{-0.65})} \quad (4)$$

and

$$r_{ND}^{\text{Fe}:\text{C}} = \frac{1}{\text{MIN}(300000, 20000 + 31805 \cdot ([\text{Fe}] - 0.125)^{-0.65})} \quad (5)$$

where $[\text{Fe}]$ is the dissolved iron concentration (nmol kg^{-1}). A threshold level representing a maximum efficiency of iron utilization is imposed, arbitrarily set at a value of $3 \times 10^5 \text{ mol C (mol Fe)}^{-1}$ (equivalent to $\sim 3.3 \mu\text{mol Fe (mol C)}^{-1}$). Assuming that there is no fractionation between the Fe and C components of POM within the euphotic zone, $\text{Fe}:\text{C}$ export production ratios for the two phytoplankton groups are set equal to these empirical cellular relationships.

Incubation and ocean patch studies have reported changes in the cellular uptake ratios of $\text{H}_4\text{SiO}_4:\text{C}$ and $\text{H}_4\text{SiO}_4:\text{NO}_3$ by HNLC-type phytoplankton assemblages upon the addition of iron^{15,16} (and in this present study). Fe-stressed diatoms are also visibly more heavily silicified^{17,18}. It has been suggested that this increase in diatom $\text{H}_4\text{SiO}_4:\text{C}$ with decreasing Fe-availability may be due to the order of cell cycle events, where silicic acid uptake only occurs in a phase just prior to cellular division¹⁹. If division is delayed through Fe-limitation, the length of time available for opal deposition is longer resulting in a higher degree of diatom silicification. If this is the case, a reasonable starting point in relating $\text{H}_4\text{SiO}_4:\text{C}$ uptake to ambient $[\text{Fe}]$ would be to assume that this ratio is proportional to Fe-stress, as defined by the reciprocal of the relevant Michaelis-Menten kinetic term

(3b). The singularity which would otherwise occur at $[\text{Fe}] = 0$ is removed by adding a fixed offset ($[\text{Fe}]_{\text{off}}$) to the value of ambient $[\text{Fe}]$. The resulting equation for the diatom uptake ratio of $\text{H}_4\text{SiO}_4:\text{C}$ is then

$$r_{\text{D}}^{\text{H}_4\text{SiO}_4:\text{C}} = r_{0,\text{D}}^{\text{H}_4\text{SiO}_4:\text{C}} \cdot \frac{K_{\text{S}}^{\text{Fe}} + ([\text{Fe}] + [\text{Fe}]_{\text{off}})}{([\text{Fe}] + [\text{Fe}]_{\text{off}})} \quad (6)$$

where $r_{0,\text{D}}^{\text{H}_4\text{SiO}_4:\text{C}}$ is the ratio of $\text{H}_4\text{SiO}_4:\text{C}$ uptake under Fe-replete conditions. Mean $\text{H}_4\text{SiO}_4:\text{C}$ ratios under Fe-replete (in patch) and Fe-deplete (out of patch) conditions observed in SOIREE were 0.19 and 0.35, respectively (see Supplementary Information part 1). Assuming a mean in patch $[\text{Fe}]$ of 1.5 nmol kg^{-1} and $0.06 \text{ nmol kg}^{-1}$ out of patch, the relative difference in observed $\text{H}_4\text{SiO}_4:\text{C}$ can be reproduced by assuming values for K_{S}^{Fe} and $[\text{Fe}]_{\text{off}}$ of 0.32 and 0.2 nmol kg^{-1} , respectively. This also gives excellent agreement with the relative ratio changes reported by ref 15. Since our biological model considers export rather than uptake, $r_{0,\text{D}}^{\text{H}_4\text{SiO}_4:\text{C}}$ is treated as a tunable parameter, incorporating the effect on the final export $\text{H}_4\text{SiO}_4:\text{C}$ ratio due to any differential recycling between opal and POM within the euphotic zone.

Remineralization within the water column

Remineralization of POM, CaCO_3 , and opal take place in the water column according to the parameterizations of ref 20 for POM and CaCO_3 , and ref 21 in the case of opal. For POM, its constituents (carbon, alkalinity, and nutrients) are remineralized in a ratio invariant with depth, and equal to the net uptake (export) ratio.

Sedimentary diagenesis

For simplicity, the system is assumed to be ‘closed’ w.r.t. H_4SiO_4 , PO_4 , and O_2 , such that POM and opal not remineralized within the water column are immediately remineralized upon reaching the sediment surface (and returned in dissolved form back to the ocean). However, to account for the process of ‘calcium carbonate compensation’²², dissolution of CaCO_3 within the sediments is represented explicitly, and proceeds according to ref 23. In this, dissolution of CaCO_3 is driven both by the degree of under saturation of the ocean waters and as a result of the respiration of POM within the sediments. There is no release of Fe from the sediments.

Iron biogeochemical cycling

Dissolved iron in the ocean is considered as a single total dissolved species which is ultimately available for biological uptake at the ocean surface. Its oceanic cycling is represented in a similar way to recent model studies^{24,25,26}. However, two major departures are made. Firstly, the action of Fe-binding ligands is not considered, so that there is no effective ‘threshold’ below which Fe cannot be scavenged. Secondly, rather than represent the scavenging of Fe with the use of a simple characteristic Fe residence time applied uniformly throughout the ocean, the scavenging rate is related directly to the flux density of settling POM. The mass

fraction of Fe in aeolian dust is assumed to be equal to the mean crustal abundance of 3.5% ²⁷. Estimates of Fe solubility range over a full 3 orders of magnitude from $<0.013\%$ to 55% ²⁸, rendering the assignment of solubilities in the model problematic. Solubility values are therefore chosen in conjunction with the Fe scavenging rate on the basis of producing a ‘reasonable’ oceanic distribution of Fe. Since the effective solubility of Fe appears to be much higher when dust is ‘wet’ rather than ‘dry’ deposited to the ocean surface and additionally increases with atmospheric processing²⁹, solubilities are allowed to differ between regions. The solubility of dust deposited to the Atlantic is therefore assumed to be lower than that to regions such as the Antarctic, which are remote from dust source areas.

Isotope fractionation

Fractionation between ^{12}C and ^{13}C within the aqueous carbonate system and during air-sea exchange follows ref 6, while during CaCO_3 formation, ref 30. Rather than adopt a fixed value associated with the biological formation of POM in the surface ocean, fractionation is dependent on the ambient concentration of $\text{CO}_{2(\text{aq})}$ ³¹. The theoretical model of refs 32 and 33 is simplified, so that the isotopic signature of POM ($\delta^{13}\text{C}^{\text{POC}}$) relative to that of $\text{CO}_{2(\text{aq})}$ ($\delta^{13}\text{C}^{\text{CO}_{2(\text{aq})}}$) is written (as ‰)

$$\delta^{13}\text{C}^{\text{POC}} = \delta^{13}\text{C}^{\text{CO}_{2(\text{aq})}} - \varepsilon_f + (\varepsilon_f - \varepsilon_d) \cdot \frac{K_Q}{[\text{CO}_{2(\text{aq})}]} \quad (7)$$

where ε_f and ε_d are the isotope fractionations (‰) associated with enzymic intercellular C fixation and $\text{CO}_{2(\text{aq})}$ diffusion respectively, and $[\text{CO}_{2(\text{aq})}]$ is the ambient concentration of $\text{CO}_{2(\text{aq})}$ (mol kg^{-1}). K_Q accounts for a variety of cellular factors, and with typical phytoplankton parameter values^{32,33} can be approximated

$$K_Q = 2.83 \times 10^{-10} - 1.79 \times 10^{-7} \cdot T + 3.17 \times 10^{-5} \cdot T^2 \quad (8)$$

where T is the temperature (K). The value of ε_f is assumed to differ between phytoplankton classes, taking values of -25% and -20% , for diatoms and non-diatoms, respectively, while ε_d is 0.7% for both classes.

Numerical scheme

Equations describing intra-ocean and ocean-atmosphere processes are solved numerically by a simple forward-time finite difference scheme with a time step of 30 days, while sediment-ocean processes are solved asynchronously on an annual basis.

Model optimization

Unconstrained model parameter values are chosen on the basis of achieving balanced model end-state ‘success’, as measured against a basket of present-day observational data. Observational constraints considered include oceanic fields of PO_4 , H_4SiO_4 , and Fe, particulate fluxes of POC and CaCO_3 (and in particular the $\text{CaCO}_3:\text{POC}$ rain ratio), and core-top CaCO_3 content. Parameter values resulting from this optimization are detailed in Table 3. Fe solubilities for

each of the surface ocean regions are listed in Table 1, giving a mean global solubility for Fe of 0.54%, close to reported estimates of 0.8-2.1%²⁸.

The value for the export Si:C ratio under Fe-replete conditions ($r_{0,D}^{H_4SiO_4:C}$) is some ~2.5 times greater than the in patch uptake ratio observed during SOIREE (see supplementary information), and about 2 times greater than that reported by ref 15. This is consistent with estimated differential recycling between particulate Si and N phases within the euphotic zone of factor 1.25 to 3.0^{34,11}.

Total POC export out of the surface boxes in the model is ~3.4 GtC a⁻¹. Correcting (for remineralization) to a reference depth in the water column of 100 m, suggests an equivalent flux of ~4.5 GtC a⁻¹. This is consistent with the range of data- and model-based estimates of 3.4 to >15.0 GtC a⁻¹³⁵. Mean ocean CaCO₃:POC is 0.20, or 0.15 when corrected to 100 m, consistent with reported estimates of 0.08-0.25^{36,37}. Global opal export is 180 Tmol a⁻¹, rising to around 200 Tmol a⁻¹ at 100 m depth, consistent with mass balance and modelling-derived estimates of 120-275 Tmol a⁻¹^{38,39,40}.

Fluxes into the system of dissolved inorganic DIC and ALK of about 11 and 22 Tmol a⁻¹, respectively, are required in order to balance burial of CaCO₃ in the deep-sea over the long-term and produce oceanic inventories consistent with pre-industrial estimates³⁷. DIC input requires an associated $\delta^{13}C$ of about 2.65‰.

References

- Keir, R. S. On the late Pleistocene ocean geochemistry and circulation. *Paleoceanogr.* **3**, 413-444 (1988).
- Munhoven, G. & Francois, L. M. Glacial-interglacial variability of atmospheric CO₂ due to changing continental silicate rock weathering: A model study. *J. Geophys. Res.* **101**, 21423-21437 (1996).
- Levitus, S., Burgett, R. & Boyer, T. World Ocean Atlas 1994 vol 3: Nutrients (NOAA Atlas NESDIS 3, US Dept of Commerce, Washington D.C., 1994).
- Mahowald, N. et al. Dust sources and deposition during the last glacial maximum and current climate: a comparison of model results with paleodata from ice cores and marine sediments. *J. Geophys. Res. - atmospheres* **104**, 15895-15916 (1999).
- Maier-Reimer, E. Geochemical cycles in an ocean general circulation model. Preindustrial tracer distributions. *Glob. Biogeochem. Cyc.* **3**, 645-677 (1993).
- Marchal, O., Stocker, T. F. & Joos, F. A latitude-depth, circulation biogeochemical ocean model for paleoclimate studies. Development and sensitivities. *Tellus* **50B**, 290-316 (1998).

Table 3 Parameter Values Resulting from Model Optimization

Parameter	Value
$U_{0,D}^{PO_4}$	3.0 $\mu\text{mol kg}^{-1} \text{a}^{-1}$
$U_{0,ND}^{PO_4}$	0.1 $\mu\text{mol kg}^{-1} \text{a}^{-1}$
$r_{0,D}^{H_4SiO_4:C}$	0.49
$r_{0,ND}^{CaCO_3:C}$	0.50
Scavenging rate constant	0.009 a ⁻¹ (mol C m ⁻² a ⁻¹) ⁻¹

- Eppley, R. W. Temperature and phytoplankton growth in the sea. *Fishery Bulletin* **70**, 1063-1085 (1972).
- Aksnes, D. L., Ulvestad, K. B., Balino, B. M., Berntsen, J., Egge, J. K. & Svendsen, E. Ecological modeling in coastal waters - Towards predictive physical-chemical-biological simulations-models. *Ophelia* **41**, 5-36 (1995).
- Egge, J. K. Are diatoms poor competitors at low phosphate concentrations? *J. Mar. Sys.* **16**, 191-198 (1998).
- Aksnes, D. L., Egge, J. K., Rosland, R. & Heimdal, B. R. Representation of *Emiliania-Huxleyi* in phytoplankton simulation-models - A 1st approach. *Sarsia* **79**, 291-300 (1994).
- Dugdale, R. C., Wilkerson F. P. & Minas H. J. The role of silicate pump in driving new production. *Deep-Sea Research I* **42**, 697-719 (1995).
- Officer C. B. & Ryther J. H. The possible importance of silicon in marine eutrophication. *Marine Ecology - Progress Series* **3**, 83-91 (1980).
- Sunda, W. G. & Huntsman, S. A. Iron uptake and growth limitation in oceanic and coastal phytoplankton. *Mar. Chem.* **50**, 189-206 (1995).
- Rue, E. L. & Bruland, K.W. The role of organic complexation on ambient iron chemistry in the equatorial Pacific Ocean and the response of a mesoscale iron addition experiment. *Limnol. Oceanog.* **42**, 901-910 (1997).
- Hutchins, D. A. & Bruland, K. W. Iron-limited diatom growth and Si:N uptake ratios in a coastal upwelling regime. *Nature* **393**, 561-564 (1998).
- Takeda, S. Influence of iron availability on nutrient consumption ratio of diatoms in oceanic waters. *Nature* **393**, 774-777 (1998).
- Hutchins, D. A., DiTullio, G. R., Zhang, Y. & Bruland, K. W. An iron limitation mosaic in the California upwelling regime. *Limnol. Oceanog.* **43**, 1037-1054 (1998).
- Leynaert, A., Nelson, A., Queguiner, B. & Tréguer, P. The silica cycle in the Antarctic Ocean - Is the Weddell Sea atypical? *Marine Ecology - Progress Series* **96**, 1-15 (1993).
- Pondaven, P., Ruiz-Pino, D., Druon, J. N., Fravallo, C. & Tréguer, P. Factors controlling silicon and nitrogen biogeochemical cycles in high nutrient, low chlorophyll systems (the Southern Ocean and the North Pacific): Comparison with a mesotrophic system (the North Atlantic). *Deep-Sea Res. I* **46**, 1923-1968 (1999).
- Archer, D, Kheshgi, H. & Maier-Reimer, E. Dynamics of fossil fuel CO₂ neutralization by marine CaCO₃. *Glob. Biogeochem. Cyc.* **12**, 259-276 (1998).
- Gnanadesikan, A. A global model of silicon cycling: Sensitivity to eddy parameterization and dissolution. *Glob. Biogeochem. Cyc.* **13**, 199-220 (1999).
- Broecker, W. S. & Peng, T.-H. The role of CaCO₃ compensation in the glacial to interglacial atmospheric CO₂ change. *Glob. Biogeochem. Cyc.* **1**, 15-29 (1987).
- Archer, D. Modeling the calcite lysocline. *J. Geophys. Res.* **96**, 17037-17050 (1991).
- Archer, D. E. & Johnson, K. A Model of the iron cycle in the ocean. *Glob. Biogeochem. Cyc.* **14**, 269-279 (2000).
- Lefèvre, N. & Watson, A. J. Modelling the geochemical cycle of iron in the oceans and its impact on atmospheric CO₂ concentrations. *Glob. Biogeochem. Cyc.* **13**, 715-736 (1999).
- Watson, A. J. & Lefèvre, N. The sensitivity of atmospheric CO₂ concentrations to input of iron to the oceans. *Tellus* **51B**, 543-460 (1999).
- Duce, R. A. & Tindale, N. W. Atmospheric transport of iron and its deposition in the ocean. *Limnol. Oceanog.* **36**, 1715-1726 (1991).
- Jickells, T. D. & Spokes, L. J. in *The biogeochemistry of iron in seawater* (eds Turner, D. & Hunter, R.) (John Wiley & Sons, Chichester, England, in press).
- Spokes, L. J. & Jickells, T. D. Factors controlling the solubility of aerosol trace metals in the atmosphere and on mixing into seawater. *Aquatic Geochem.* **1**, 355-374 (1996).
- Mook, W. G. ¹³C in atmospheric CO₂. *Netherlands Journal of Sea Research* **20**, 211-223 (1986).
- Hofmann, M., Broecker, W. S. & Lynch-Stieglitz, J. Influence of a [CO_{2(aq)}]¹²C dependent biological C-isotope fractionation on glacial ¹³C/¹²C ratios in the ocean. *Glob. Biogeochem. Cyc.* **13**, 873-883 (2000).

32. Rau, G. H., Riebesell, U. & Wolf-Gladrow, D. A model of photosynthetic ^{13}C fractionation by marine phytoplankton based on diffusive molecular CO_2 uptake. *Mar. Ecol. Prog. Ser.* **133**, 275-285 (1996).
33. Rau, G. H., Riebesell, U. & Wolf-Gladrow, D. $\text{CO}_{2\text{aq}}$ -dependent photosynthetic ^{13}C fractionation in the ocean: A model versus measurements. *Glob. Biogeochem. Cyc.* **11**, 267-278 (1997).
34. Dugdale, R. C. & Wilkerson F. P. Silicate regulation of new production in the equatorial Pacific upwelling. *Nature* **391**, 270-273 (1998).
35. Ducklow, H. W. Ocean biogeochemical fluxes - New production and export of organic-matter from the upper ocean. *Rev. Geophys.* **33**, 1271-1276 (1995).
36. Broecker, W. S. & Peng, T.-H. *Tracers in the sea* (eds Broecker, W. S. & Peng, T.-H. (Lamont-Doherty Geological Observatory, Palisades, New York, 1982).
37. Yamanaka, Y. & Tajika, E. The role of the vertical fluxes of particulate organic matter and calcite in the oceanic carbon cycle: Studies using an ocean biogeochemical general circulation model. *Glob. Biogeochem. Cyc.* **10**, 361-382 (1996).
38. Archer, D., Winguth, A., Lea, D. and Mahowald, N. What caused the glacial/interglacial atmospheric $p\text{CO}_2$ cycles. *Rev. Geophys.* in press.
39. Heinze, C., Maier-Reimer, E., Winguth, A. M. E. & Archer, D. A global oceanic sediment model for long-term climate studies. *Glob. Biogeochem. Cyc.* **13**, 221-250 (1999).
40. Tréguer, P., Nelson, D. M., Van Bennekom, A. J., DeMaster, D. J., Leynaert, A. & Queguiner, B. The silica balance in the world ocean - A reestimate. *Science* **268**, 375-379 (1995).